Segregation Phenomena at Thermally Grown Al_2O_3/Alloy Interfaces

P.Y. Hou

Materials Sciences Division, Lawrence Berkeley National Laboratory, Berkeley, California 94720; email: pyhou@lbl.gov

Annu. Rev. Mater. Res. 2008. 38:275–98

First published online as a Review in Advance on March 14, 2008

The *Annual Review of Materials Research* is online at matsci.annualreviews.org

This article's doi: 10.1146/annurev.matsci.38.060407.130323

1531-7331/08/0804-0275$20.00

Key Words

oxidation, sulfur, chromium, platinum, reactive element

Abstract

Experimental results on S segregation at growing Al_2O_3/alloy interfaces are reviewed for binary FeAl, NiAl alloys, and ternary alloys with additions of Cr, Pt, or a reactive element, such as Zr, Hf, or Y. The segregation behavior is thermodynamic in nature, but the segregation energy can change not only with alloying elements but also with oxidation time and temperature as the oxide growth process changes. Although reactive elements are capable of eliminating interfacial S segregation, they do not stop such segregation to alloy surfaces. The segregation of a reactive element at the interface further strengthens the interfacial bonding. Cosegregation of S and Cr can occur, resulting in higher levels of S at the interface. Pt usually suppresses S segregation, but this effect can be easily overwhelmed by S-Cr cosegregation. Synergisms between alloying elements and how they affect segregation, as well as the relationship between segregation and the oxidation process, are areas that demand further investigation.

INTRODUCTION

The concentration of sulfur, a common impurity in metals and alloys, usually ranges from tens of parts per million in Fe-based alloys to a few parts per million in NiAl. Even at such low levels, S segregates strongly to surfaces, where diffusion from the bulk to the surface is rapid, especially at elevated temperatures (1). At equilibrium, the surface concentration of S depends on the temperature, the amount in the alloy, and the segregation energy. S segregates to grain boundaries of metals and alloys, causing grain boundary embitterment (2–4). For a given metal or alloy and its S content, the degree of segregation to grain boundaries is often less than that to the free surface (5).

It was proposed that, when an alloy is oxidized at elevated temperatures, S segregates to the oxide/alloy interface formed by oxidation and weakens the interfacial bonding, making the oxide scale nonadherent (6). Because all alloys operated at high temperatures rely on a thermally grown oxide (TGO) film, or scale, that is slow growing and adherent to protect it from continued oxidation and degradation, this possible S segregation and interface-weakening phenomenon is of great technological importance. The proposal gained much support after Smialek (7, 8) demonstrated that removing S from the alloy, often by a high-temperature H_2-annealing heat treatment, can increase significantly the spallation resistance of the scale during cyclic oxidation. However, the H_2 annealing also removes other nonmetallic impurities, such as C, and reduces porosity at the oxide/alloy interface, making it difficult to evaluate the true effect of S on scale adhesion base on oxide spallation data. Several other questions also remain. The most fundamental one is whether segregation of a large and negatively charged S atom to an oxide/alloy interface is thermodynamically favorable (9). Furthermore, because of the dynamic nature of the growing interface under consideration, where new oxides are continually formed and internal stresses generated, it is not clear if S or any other impurities would be present solely as a result of thermodynamic segregation. In other words, factors that affect segregation at a growing oxide/alloy interface may be different from those governing segregations to surfaces and grain boundaries.

This paper reviews results and the current understanding of the segregation phenomena at the interfaces formed between alloys and their TGO scales. Whenever possible, segregation to free surfaces is compared, and the effect of interface S on scale adhesion is addressed. This review focuses on Al_2O_3/alloy systems because the majority of works concerning interfacial segregation have been performed on alloys whose TGO is Al_2O_3; only a few were done with Cr_2O_3 scales on Cr (10, 11) or binary Ni-Cr (12) and Fe-Cr (13) alloys. Because the particular interface in question is that formed by oxidation, a brief background on the development and growth of Al_2O_3 scales is first given. This is followed by a section describing the experimental techniques typically employed for these types of interfacial studies. Discussions on S segregation begin with simple binary Fe-Al and Ni-Al alloys, and then the effects of common alloying additives on segregation are examined. Such additives include Cr, Pt, or reactive elements (REs), such as Hf, Zr, and Y, which have higher oxygen affinity than the scale-forming element, namely, Al.

GROWTH AND DEVELOPMENT OF ALUMINA SCALES ON ALLOYS

There are two main types of Al_2O_3-forming alloys: the aluminides, such as FeAl and NiAl, and the MCrAl-type alloy that is the base of superalloys, where M represents the base metal and can be a mixture of Fe, Ni, and Co. For the aluminides, approximately 19–22 at% Al is needed to achieve the selective oxidation of Al to develop a protective Al_2O_3 scale and to suppress the oxidation and growth of base metal oxides (14). The addition of 18–20 at% Cr in MCrAl-type alloys reduces the critical Al concentration to no more than 10 at% (15, 16).

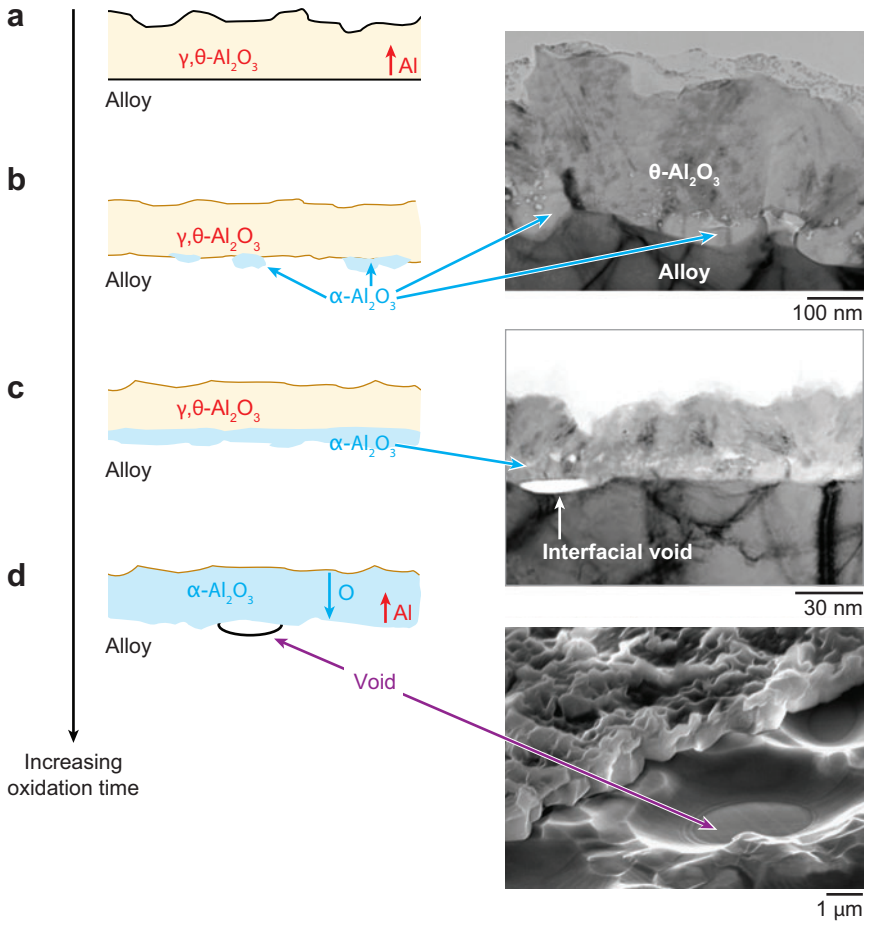

Figure 1

The sequences of Al_2O_3 scale development on alloys oxidized at high temperatures. (*a*) Transition alumina forms initially, and its growth is dominated by Al outward transport. (*b*) α-Al_2O_3 grains nucleate at the oxide/alloy interface. (*c*) A complete layer of α-Al_2O_3 establishes at the interface; interfacial voids often develop on alloys not containing a reactive element. (*d*) The entire scale transforms to α-Al_2O_3, and its growth is dominated by oxygen inward diffusion; interface voids can grow to considerable sizes.

The sequence of Al_2O_3 scale development is illustrated in **Figure 1**. The first formed layer, usually referred to as transition aluminas, consists mainly of the cubic θ phase (17, 18), γ phase (19–23), or a mixture of the two phases (24–26). This initial layer has a cube-on-cube orientation relationship with the alloy, whereas the degree of preferred orientation decreases with oxidation time (19, 21, 26, 27). The thermodynamically most stable hexagonal α-Al_2O_3 nucleates later at the transition alumina/alloy interface (**Figure 1*b***) with a random orientation (21, 23). Limited high-resolution transmission electron microscopy (TEM) studies have shown that the interface between the transition alumina and the alloy is coherent but becomes incoherent once α-Al_2O_3 nucleates (28). The α nuclei eventually impinge and develop into a complete layer above the alloy (**Figure 1*c***). The subsequent scale-thickening rate becomes dominated by the slow growth of this α layer, whereas the initially formed transition alumina transforms to the α phase with time

(**Figure 1*d***). The development of α-Al_2O_3 is more rapid at higher temperatures (19) and easier with the presence of Cr (29) and/or Fe (26, 30) in the alloy. Because Cr_2O_3 and Fe_2O_3 have the same corundum structure as α-Al_2O_3, they may serve as templates that facilitate the nucleation and growth of the α phase (29, 30). The transition alumina grows predominantly by Al outward transport (31, 32), but the α-Al_2O_3 grows predominantly by oxygen inward transport, with a nontrivial amount of Al outward diffusion (33), unless a RE is present, in which case Al outward transport is greatly reduced (34).

The initial θ-Al_2O_3 layer is under high compression, approximately 300 MPa (18). The first nucleated α-Al_2O_3 grains or patches are under tension, which can be as high as 400–600 MPa, owing to a ~5% volume shrinkage associated with the θ-to-α transformation (18, 35, 36). Without the presence of any RE, this tensile stress quickly relaxes, and compression builds up within the α layer as oxidation continues (18, 36).

Extensive void formation at scale/alloy interfaces is often observed without the presence of any RE or Pt, particularly on Ni and Fe aluminides (37, 38). These voids deepen into the alloy, often showing faceted faces and distinct shapes that are associated with the alloy grains (**Figure 1*d***). The void faces are essentially free surfaces under the growing scale. The amount of S, or other segregand, on them provides valuable information on surface segregation that can be directly compared with what is present at the interface under the exact same oxidation condition.

EXPERIMENTAL METHODS

Direct characterization of the interfacial chemistry using conventional surface techniques, such as X-ray photoelectron spectroscopy (XPS) and Auger electron spectroscopy (AES), is possible only through ultrathin oxide films, ~0.5 nm, formed at ambient temperatures (39). For thicker films, the interface is buried to surface investigations, so analysis will have to occur either by stripping off the oxide film or by cross-sectioning. Furthermore, unlike surface segregation studies, in which the amount of segregand can be determined in situ at elevated temperatures, studies of interface segregation so far have been performed after cooling the oxidized sample to room temperature. AES depth profiling has been attempted (9), but owing to the roughness of the interface and the narrow distribution of segregated S there, detection is not always possible. More sensitive techniques, such as secondary ion mass spectrometry (SIMS), improve the detectability (40). However, neither of these methods reveals the interface microstructure, so one cannot distinguish whether the detected S is from intact interfacial areas or from interfacial voids.

If the oxide film can be removed from the alloy in ultrahigh vacuum (UHV), then the alloy side of the sample can be easily analyzed through the use of a scanning Auger microprobe, whereby images produced by the secondary electrons allow the probe to be placed on known microstructures. To remove the oxide film, thin strips of oxidized alloy are bent in UHV, and then the exposed alloy is analyzed by a conventional (~0.5–1-μm probe size) scanning Auger probe (41–43). Alternatively, the oxidized sample surface can be scratched with a Vickers microindenter mounted on a linear translator inside the UHV chamber (11, 12). Scratches made this way, when applied with sufficient load, cause pieces of the oxide scale around the scratch mark to spall, hence exposing the scale/alloy interface (see **Figure 2** for an example). The exposed alloy areas can then be analyzed via AES, whether on oxide-imprinted areas, where the oxide has been in contact with the alloy prior to the scratch, or on the surface of interfacial voids. The advantage of the scratch over the bend technique is that sample thickness is not a limit. Furthermore, oxide pieces that spall from the scratch motion mostly remain on the sample surface, and some of them are flipped over, allowing the oxide side of the interface (the scale underside) to be examined. These locations usually consist of only oxygen and Al. In other words, all segregands reside on the alloy side after scale spallation. The only

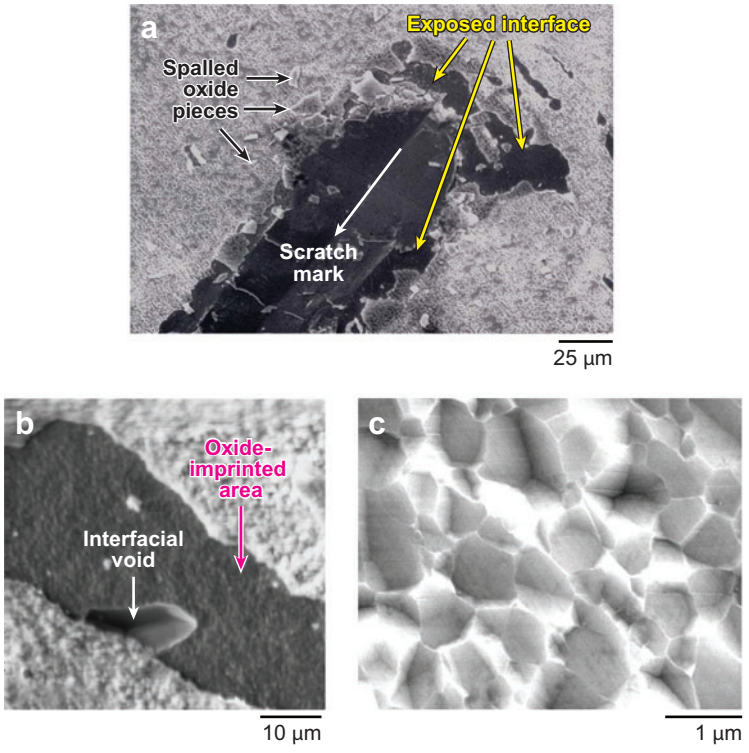

Figure 2

Examples of scratch-induced oxide spallations that expose the interface for subsequent AES analysis. (*a*) A scratch is made in ultrahigh vacuum on the surface of an oxidized sample, causing oxide fracture and spallation around the scratch mark. Analysis can be done on the alloy side as well as the oxide side of the interface. (*b*) Magnified view of a typical alloy interface region, showing one interfacial void and the surrounding oxide-imprinted area, where the oxide was in contact with the alloy prior to spalling. (*c*) Magnified view of the oxide-imprinted area, showing facets marked by α-Al_2O_3 grains.

exception is when the S segregation is multilayered (44); then, occasionally, small amounts of S can be detected on the oxide underside, but the concentration is still less than that found on the alloy.

The degree of scratch-induced oxide spalling can be characterized to provide a measure of the interface strength. For strong interfaces, those often formed on RE-containing alloys, the TGO spalls at only a few small areas adjacent to the scratch, making the analysis more difficult than for a weak interface, where large areas of the interface are exposed. TEM observations and scanning transmission electron microscopy (STEM) analysis across an oxide/alloy interface are most suitable for strong interfaces. Furthermore, the technique undoubtedly examines intact interfaces, where porosity, even if nanometers in size, can be easily distinguished (10, 45–48). Unfortunately, detection of S is usually difficult, partly owing to its desorption under the electron beam (46) and partly owing to the low levels segregated at the interface. Experiences indicate that the interface S content has to be higher than ~0.4 monolayer (estimated from AES results) before S can be detected by STEM (47, 48). A few studies have reported the detection of S at the oxide/alloy interface, using energy-dispersive X-ray analysis (EDS) on metallographically polished cross sections (49, 50). However, in both cases, the alloy contains high levels of S, and small amounts of sulfides may be formed at the interface.

Most of the results presented in this review are obtained from the scratch method with a conventional AES operating at 10 kV. One sample, for comparison, has been examined through the use of a field emission AES that has a much finer probe size, 30 nm, allowing analyses to be made on individual oxide-imprinted facets on the alloy surfaces (51). A few alloys have also been studied via the scanning μXPS beamline at the Advanced Light Source in Lawrence Berkeley National Laboratory, with an approximate spot size of ~2 × 2 μm, to distinguish the chemical states of the segregated S (52).

SEGREGATION AT ALUMINA/BINARY ALLOY INTERFACES

Interfacial Sulfur Buildup with Oxidation Time

The amount of S present at an Al_2O_3/alloy interface as a function of oxidation time has been examined for Fe-40Al through the use of conventional as well as field emission AES (51) and for several batches of Ni-40Al through the use of conventional AES (53, 54). Most of the NiAl alloys have only 3–4 ppm S (normal purity), but one was deliberately doped to achieve a bulk S content of 36 ppm (S-doped sample). Both types of FeAl and NiAl alloys are single-phase β-aluminide. In all cases, S was the only impurity found at the interface. Results are summarized in **Figure 3**,

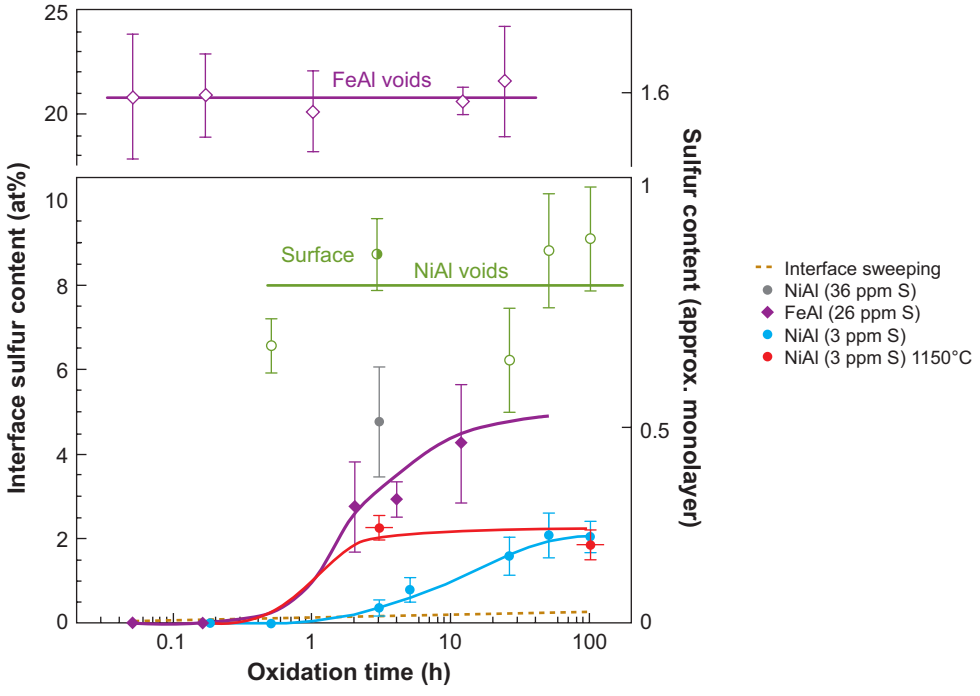

Figure 3

Summary of AES analysis of the interface S content on Fe–40 at% Al (FeAl) and Ni–40 at% Al (NiAl) alloys as a function of oxidation time at 1000°C. A few samples were oxidized at 1150°C. The bulk S concentration, in parts per million, is noted for each batch of alloy. Open symbols represent the amount of S found on void surfaces, and closed symbols the amount of S on oxide-imprinted interfacial areas. The data marked as surface is the amount of S segregated on Ni-40Al when the alloy is heated in vacuum at 1000°C. Interface sweeping represents the amount of S that would accumulate at an advancing interface due entirely to scale inward growth.

in which each data point is obtained from one specific sample isothermally oxidized for a given time and then air quenched. Most oxidations were performed at 1000°C, except for a few carried out at 1150°C. The S concentration in atomic percent, calculated through the use of tabulated AES sensitivity factors (55), represents the amount of S present within approximately the top four atomic layers. Because AES depth profiling shows that S is located at the very surface, a layer model was used to determine the coverage in monolayer from the degree of attenuation of the base metal signals (55), i.e., that of Fe or Ni. **Figure 3** presents data from void surfaces and from oxide-imprinted areas, where the oxide was in contact with the alloy prior to spallation; typical microstructures of these interfacial voids and α-Al_2O_3 imprints are seen in **Figures 1*d*** and **2*b***.

The segregation behavior found on void faces is indeed similar to that on free surfaces. The data labeled as surface on **Figure 3** are obtained at 1000°C after heating one normal-purity Ni-40Al alloy through the use of a hot-stage AES (56). The amount of S segregated onto the surface at 1000°C compares well with the amount of S found on interfacial void faces after cooling. The large data scattering on the voids arises from segregation dependence on crystallographic orientation (54). On the iron aluminide, the void S levels are much higher than on NiAl, owing to a cosegregation of S and Al (51). Although Al and S do not actually cosegregate to Fe surfaces, as determined by quantitative low-energy electron diffraction (LEED) analyses (57), a chemical disorder occurs within the subsurface layers, with Al substituting for the Fe atoms, which can explain the apparent Al-S cosegregation detected by AES. On Ni-based alloys, Al-S cosegregation does not take place (58).

The amounts of S present between the alloy and the oxide, or at true interfaces, are always noticeably less than those found on void faces. Furthermore, whereas void faces are saturated with S at an early time, <3 min for Fe-40Al and <30 min for Ni-40Al, none can be detected at true interfaces until the development of a complete layer of α-Al_2O_3, the time for which is shorter for the Fe-based alloy and shorter at higher oxidation temperatures, in accordance with the literature records on alumina development and transformation outlined in the previous section. Once the α-Al_2O_3 layer is formed, the S concentration at the interface begins to increase and then slowly approaches a saturation level. The observed delayed buildup at true interfaces cannot be related to S diffusion rates in the alloy because the void faces are already fully covered. One possible explanation is that the detected S is a result of interface sweeping, such that, as the oxide grows inward with time, S in the alloy becomes accumulated at the interface as the interface advances. From the growth rate of the α-Al_2O_3, and if one assumes 100% scale inward growth and 5 ppm S in the bulk, the amount of S thus accumulated at the interface is seen to be minute (see **Figure 3**). The concentration is too low to account for the amount of S detected; therefore, S must have segregated to intact interfaces. The results presented in **Figure 3** show that this segregation is dependent not only on the type of oxide present at the interface but also on the amount of S in the bulk, with more segregated at higher bulk S concentrations.

The dependence of interface S content on the amount of S in the bulk is in agreement with formulations developed for thermodynamic segregations, in which the amount of segregated solute, X_1^{ϕ}, is directly related to the amount of solute in the bulk, X_1^{B}. The segregation equation for an ideal binary solid solution is given by the Bragg-Williams expression (59)

$$\frac{X_1^{\varphi}}{1-X_1^{\varphi}} = \frac{X_1^{B}}{1-X_1^{B}} \exp\left(\frac{\Delta G + 2\Omega_{12}(X_1^{\varphi} - X_1^{B})}{RT}\right), \qquad 1.$$

where $\Delta G = \mu_1^B - \mu_1^{\phi} - \mu_2^B + \mu_2^{\phi}$ is the segregation energy and the μs denote the ground-state chemical potentials of the solute (1) or the solvent (2) at the surface (ϕ) or in the bulk (B). Ω_{12} is the interaction coefficient between the solvent and the solute. Ω_{12} is positive if the interaction is attractive and negative if the interaction is repulsive. If it were zero, the above equation would

reduce to the well-known Langmuir-McLean expression. The segregation phenomenon discussed here involves multicomponents and therefore is much more complicated than described by the above equation. However, the fundamental concepts are analogous, so this formulation can serve to illustrate the important parameters and their relationships. For example, if one treats S as the only segregand (the solute) and the Ni-40Al alloy as the solvent and considers that $\Omega_{12} = 0$, the segregation energy, ΔG, will be -120 kJ mol^{-1} to account for 2% and 5% of segregated S, with 3 ppm and 36 ppm S in the alloy, respectively. This level of ΔG agrees quite well with the segregation energy of S on Ni, at -135 kJ mol^{-1} (60). Because segregation to grain boundaries is usually less favorable than that to free surfaces (5), the same can be expected for interfaces. The calculated 120 kJ mol^{-1} (1.3 eV per atom) is also in close agreement with the value determined from first-principles calculations, which reveal that the segregation energy for S at γ-Ni(Al)/Al_2O_3 interfaces ranges from 0.18–1.26 eV per atom, depending on the segregation site and the type of interface (61).

According to the segregation equation, less segregand should be present at higher temperatures, but this is contrary to the results shown in **Figure 3**, where the steady-state S content on Al_2O_3/NiAl is the same at 1000°C and 1150°C. To achieve the same level of segregation at the Al_2O_3/NiAl interface at 1150°C, the ΔG must be -140 kJ mol^{-1}, which is lower than that at 1000°C. Thus, S segregation is more favorable at interfaces grown at higher oxidation temperatures. Because oxidation involves many temperature-dependent processes, such as material transport and stress generation and relaxation, it is very likely that the interface atomic structure developed at different temperatures varies to an extent as to alter the segregation energy. Similar observations have been made at alloy grain boundaries, where the extent of solute segregation often depends on the boundary structure (62–64). Limited high-resolution TEM studies have shown that the interface between the transition alumina and NiAl is coherent but the interface between the α-Al_2O_3 and the alloy is incoherent (28). If the extent of segregation were a strong function of interface coherency, or atomic structure, it would be consistent with these TEM observations that S is not detected initially at transition alumina/alloy interfaces but begins to appear only after α-Al_2O_3 forms. Note that the interface between the alloy and the first formed, isolated α-Al_2O_3 grains is free from S. S is detected only after a complete layer of α-Al_2O_3 grains is established at the interface. It is possible that the higher interfacial stress that develops after a complete α-Al_2O_3 layer is established (18) causes the oxide to lose coherency with the underlying alloy, allowing S to segregate. Further changes at the interface, probably due to continued stress generation and relaxation processes, may allow more S to segregate until a steady-state level is reached; this steady-state level is similar to the steady-state growth stress level found through in situ X-ray diffraction (65). Therefore, although thermodynamic driving forces dictate interfacial S segregation, the dynamic nature of the TGO/alloy interface may cause the segregation energy to change with time and temperature as the interface structural changes.

Relationship between Interface Sulfur Content and Oxide Adhesion

A few mechanical testings on the strength of diffusion-bonded metal/sapphire interfaces have demonstrated detrimental effects of S on the interfacial fracture toughness (66–68). Similar results on TGO/alloy interfaces are scarce (69), owing to difficulties in examining crack propagations at the buried interface. A tensile pull test, in which a stub is placed on the oxidized sample surface through the use of an adhesive, has been used to evaluate the strength of Al_2O_3/NiAl interfaces (53). **Figure 4** shows the reduction of interface strength with increasing S content at the Al_2O_3/Ni-40Al interface. A very fast drop in strength occurs within the first 1 at% (~0.1 monolayer) of S coverage. Afterward, the strength decreases much more slowly with further S buildup. Similar results

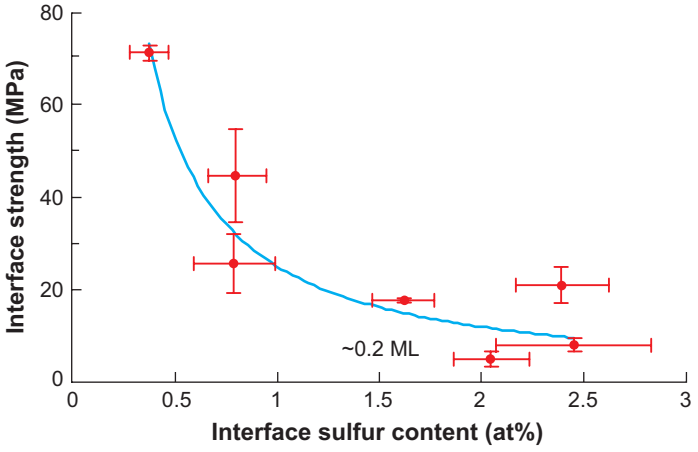

Figure 4

Relationship between interface strength (determined by a tensile pull test) and the interface S content (evaluated by AES after oxide removal in ultrahigh vacuum). ML denotes monolayer.

using first-principles calculations have recently reported that the work of separation, W_{sep} (in J m^{-2}), for Al_2O_3/γ-Ni(Al) decreases linearly with interface S coverage up to 0.4 monolayer but that further S buildup shows little or no effect on the W_{sep} (61). The major difference between the two sets of data (experiments versus calculations) is the maximum S content needed to weaken the interfacial strength most severely (0.1 monolayer versus 0.4 monolayer). One obvious cause for this discrepancy should be related to the presence of voids that form at the Al_2O_3/alloy interface during oxidation. These voids are defects that can greatly deteriorate the interfacial strength (53), but none of them are included in the calculation. The calculations were performed on γ-NiAl, whereas the experimental work was carried out on the β phase; however, the alloy phase difference should not have been an important factor because a similar degree of S segregation was also seen experimentally on γ-NiAl and is equally detrimental to the interfacial strength.

Dependence of Sulfur Segregation on Alloy Stoichiometry

Although S was readily found at α-Al_2O_3/Ni-40Al interfaces, no S could be detected when the alloy was the stoichiometric NiAl, i.e., Ni-50Al, containing 3–4 ppm S (53). Several batches of Ni50Al alloys were tested at 1000°C, 1100°C, and 1150°C for up to several hundred hours, but the interface was always free from S, with occasional B and/or P segregation. This lack of S at the interface is not restricted by S diffusivity in the alloy because plenty of S is detected on nearby void faces, as shown in **Figure 5**. The amount of S segregated to void faces is highly dependent on their crystallographic orientation; the behavior is similar to that found on Ni-40Al alloys. On the void bottom seen in **Figure 5**, the S content is ~6 at%, but that on the sides is only ~1.6 at%. One void at the lower right corner of **Figure 5*b*** does not show any S signal because that surface is still covered with C. Because S bulk diffusion in stoichiometric NiAl is nearly one order of magnitude slower than in Ni-40Al (54), as Ni is in NiAl (70) owing to strong variations of defect concentrations with composition, the first segregand on the void faces of Ni-50Al is actually C (54). S replaces the C with time, which is shorter at higher temperatures. This replacement found at void faces is similar to that observed with C and S segregation to Ni surfaces (71, 72).

To study further the effect of stoichiometry on the amount of S segregation at Al_2O_3/NiAl interfaces, Al-rich β-phase Ni-55Al, γ′-Ni-25Al, and γ/γ′-Ni-22Al alloys were oxidized between 1000°C and 1150°C after an α-Al_2O_3 layer was well established at the scale/alloy interface, and then the interface chemistry was investigated. These results are presented in **Figure 6**, which

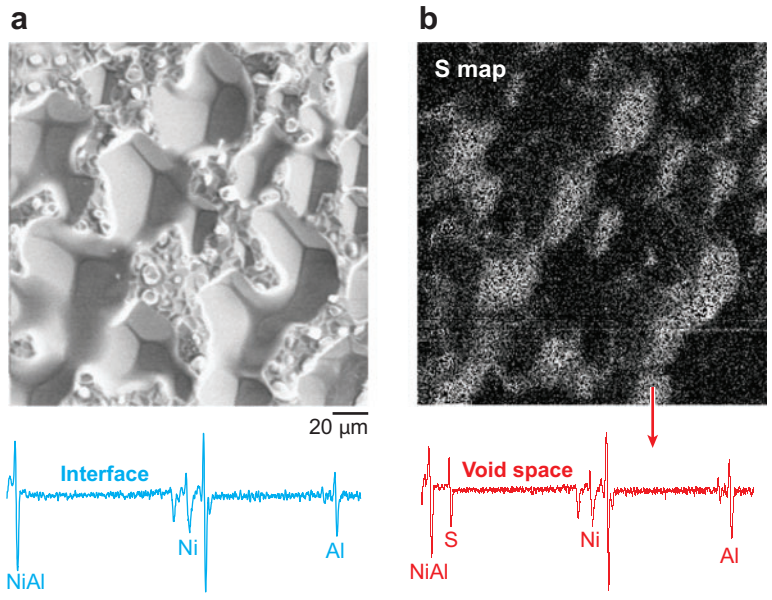

Figure 5

SEM micrograph (*a*) and associated AES S map (*b*) of the alloy side of the interface from a Ni–50 at% Al sample oxidized at 1100°C for 100 h. S is present on void faces, with different levels on different orientations, but the interface is clean, as illustrated by corresponding AES surveys.

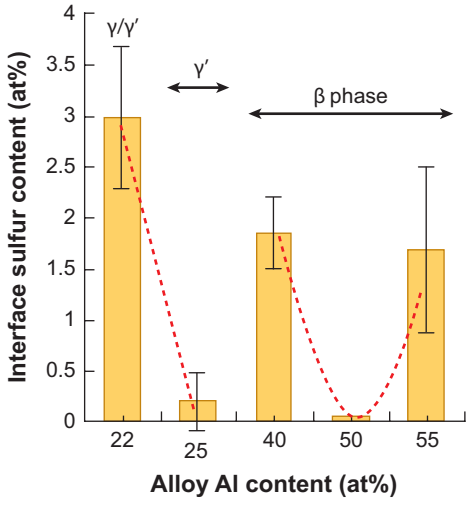

Figure 6

Variation of interface S content with NiAl alloy composition. Tested samples were oxidized between 1000°C and 1150°C for up to a few hundred hours. The level of S segregated at interfaces of ordered alloys, the γ′ and the stoichiometric β phases, is barely above background but ranges from 2–3 at% on other compositions.

shows that S is present on all oxide/alloy interfaces except for the stoichiometric β and γ′ alloys, for which the interfacial S content is only that of the background level or barely above background.

The growth processes of α-Al_2O_3 on all these NiAl alloys do not appear to be significantly different, so the observed dependence on alloy stoichiometry, in that significantly less S segregates when the alloy is an ordered phase, seems to suggest again that interfacial segregation is thermodynamic in nature. According to Equation 1, the segregation energy, $\Delta G = \mu_1^B - \mu_1^\phi - \mu_2^B + \mu_2^\phi$, is a function of the chemical potentials of the solute and solvent in the bulk and at the surface. Changes in any of the four terms can affect the degree of segregation. Because the ordered β-NiAl phase has lower surface energies than does the Ni-rich Ni40Al (73), surface segregation of S should be less favorable on the Ni-50Al. Indeed, in situ AES performed at 1000°C did show significantly less S surface segregation on Ni-50Al than on Ni-40Al (56). Less interfacial S segregation can be expected if interface energies are similarly affected. Furthermore, the chemical potentials of the solute and the solvent in the bulk, μ_1^B and μ_2^B, respectively, should be different in ordered versus disordered alloys.

EFFECT OF ALLOYING ELEMENTS ON INTERFACIAL SEGREGATION

Chromium

Cr is often added in alloys to assist the development of Al_2O_3 scales, so the alloy Al level can be kept low to maintain the alloy strength. The usual MCrAlX-type alloys are the bases for superalloys, in which M can be Fe, Co, Ni, or a mixture of the three and the X represents a number of alloying elements, such as Ti, Mo, W, Ta, Y, or Hf (74). For intermetallic alloys, small amounts of Cr are usually added to improve their mechanical properties (14).

The amount of interface S on intermetallic FeAl (**Figure 3**), even near saturation, is less than 5 at%, or ∼0.5 monolayer. However, where Cr is present (as in MCrAl-type alloys, in which the Cr concentration ranges from 15–25 at%), the amount of S at the interface is much higher, as seen in **Figure 7**. The faster buildup compared with Fe-40Al is due to the more rapid establishment of α-Al_2O_3 on the FeCrAl-type alloys. The S concentration quickly reaches a steady-state level that is close to two monolayers, and the segregation process is independent of the oxidation temperatures (between 900°C and 1100°C) or the sample cooling rates, the latter of which vary by $>10^3$ °C s^{-1} for furnace cooling and water quenching.

Besides S, C and Cr are also enriched at the Al_2O_3/FeCrAl interface (**Table 1** shows their levels). Other researchers (41, 43) have reported similar enrichments, although the elemental compositions are not as well quantified. The C in this case is not a result of vacuum or surface contamination (12, 43) but segregated mainly during cooling (44). The dependence of segregands on cooling rates, seen in **Table 1**, clearly indicates that all the detected S is present at the interface during oxidation; Cr is enriched at the oxidation temperature as well but more diffuse to the interface during cooling. Probably all the C at the Al_2O_3/FeCrAl interface resulted from diffusion during cooling because no C enrichment is found at the Al_2O_3/NiCrAl interface, where C diffusion in the fcc Ni-based alloy is much slower than that in bcc iron (75). The driving force for C diffusion to the interface should be the presence of interfacial excess of Cr, owing to the tendency for Cr carbide formation. Small Cr carbide particles have indeed been detected at alumina/FeCrAl interfaces, and the quantity increases with decreasing cooling rate (76). With lower S content in the alloy, the levels of S, Cr, and C concentrations found at alumina/FeCrAl interfaces after cooling to room temperature are also lower (**Table 1**). The concomitant increase and decrease of S and Cr, which are directly demonstrated by comparing the AES peak height ratios of S/Fe

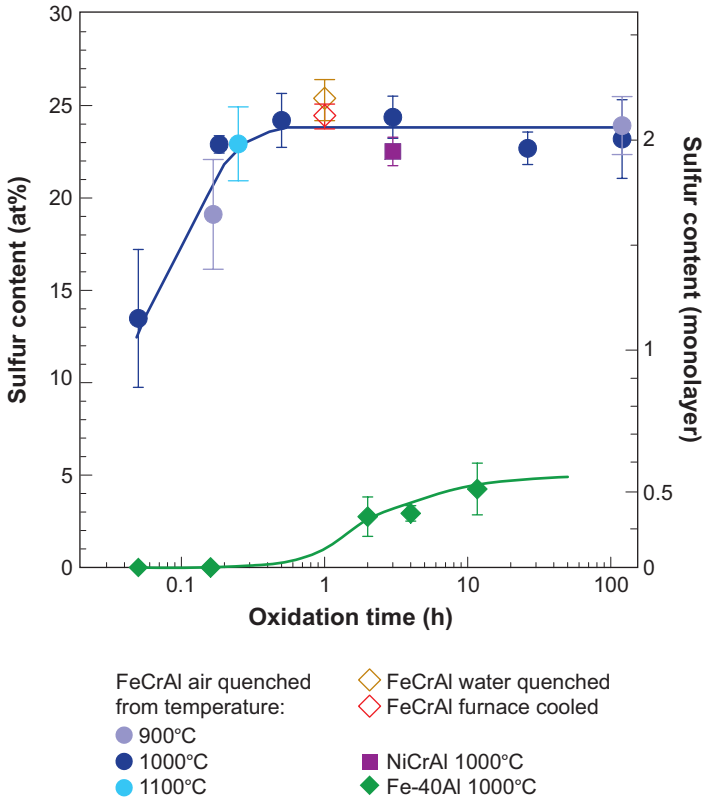

Figure 7

S buildup at Al_2O_3/Fe-18Cr-10Al (at%) interfaces as a function of oxidation time. Most samples were oxidized at 1000°C, and a few were oxidized at 900°C or 1100°C, followed by fast cooling in air (~4°C s^{-1}). Two samples were cooled with different rates (water quenched at ~140°C s^{-1} and furnace cooled at ~0.07°C s^{-1}). Results for Fe-40Al are included for comparison. One data point for a Ni-14Cr-24Al (NiCrAl) alloy is also included.

and Cr/Fe (**Figure 8**), suggest their cosegregation to the interface during oxidation. The same straight-line relationship can also be made for Cr and C (44).

The positive interaction of S with Cr, with Ω_{12} in Equation 1 greater than 0, can increase the segregation coverage such that saturation is more easily achieved and becomes less sensitive to temperature changes (77). Studies using AES and LEED have reported similar occurrences on free surfaces for Fe-Cr (78) and Fe-Cr-Ni (79) alloys, in which S and Cr cosegregate to form a two-dimensional surface structure at 750–900°C; these studies also showed similar Cr-C cosegregation at temperatures less than 750°C (78). Furthermore, there are qualitative indications that S and Cr cosegregate to the surface of a FeCrAl alloy when this alloy is heated in vacuum at 900°C (43). At the grain boundaries of a Ni-20Cr alloy, cosegregation of S and Cr caused the boundaries to be heavily decorated with Cr sulfide particles (58).

The arrangement of the segregated S, Cr, and C at the alumina/FeCrAl interface cannot be fully realized by the AES results but can be better understood through depth profiling of the segregand region. **Figure 9*a*** presents such a profile with μXPS examinations through a FeCrAl surface after Al_2O_3 scale removal in vacuum. The figure shows that the segregated elements, i.e., S, Cr, and C, are concentrated at the surface region, where two regimes can be distinguished. The

Table 1 Summary of elemental concentration at Al_2O_3/MCrAl alloy interfaces determined by AES (in at%)

Alloys	Saturation level at Al_2O_3/alloy interfaces			Bulk Cr content
	S	C	Cr	
Fe-18Cr-10Al (32 ppm S)				16.1 ± 1.6
Water quenched	25.3 ± 1.1	12.0 ± 2.7	19.3 ± 1.4	
Air quenched	23.7 ± 1.6	21.1 ± 2.4	27.1 ± 2.2	
Furnace cooled	24.2 ± 0.7	25.3 ± 1.9	27.5 ± 5.8	
Fe-18Cr-10Al (2 ppm S)				14.3 ± 0.6
Air quenched	11.7 ± 1.4	10.1 ± 1.3	18.8 ± 1.1	
Ni-14Cr-24Al (7 ppm S)				
Air quenched	22.5 ± 0.8	0.8 ± 1.6	20.8 ± 3.8	

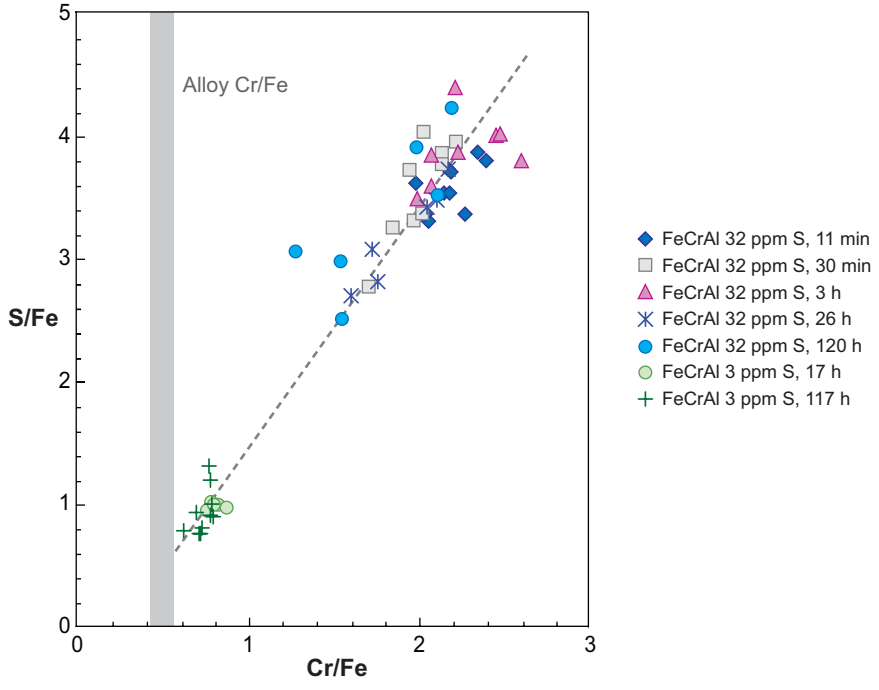

Figure 8

Relationship between S and Cr segregated at Al_2O_3/FeCrAl interfaces. AES peak height ratios with Fe are used to normalize the S and Cr contents. Data from two Fe-18Cr-10Al samples with different bulk S levels and oxidized at 1000°C are presented. Different symbols represent different oxidation times that are greater than 10 min, but time is not a factor because saturation was already reached. The straight-line relationship indicates that S and Cr cosegregate.

outer one, defined by a narrow and sharp S peak, is heavily enriched with S. Immediately beneath the S enrichment, the Cr and C concentrations reach their maxima; both concentrations then decrease slowly into the alloy, suggesting sluggish diffusion, which is consistent with the above conclusion about Cr and C diffusing to the interface during cooling. All the detected S is present as sulfides that peaked at energies between 161 eV and 161.6 eV. The C is a carbide, and the Cr,

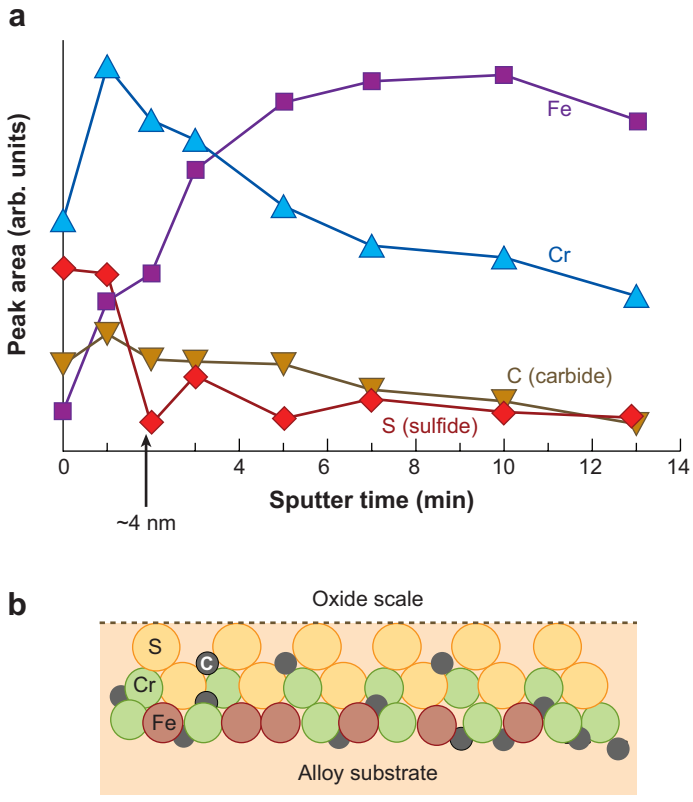

Figure 9

(*a*) Depth profiles through a Fe-18Cr-10Al surface after its TGO was removed in vacuum. Ar was used as the sputtering source and μXPS as the surface probe. S, Cr, and C all segregated at the interface; S was above the Cr and C layers. (*b*) A simple schematic illustrates the possible distribution of these segregated elements.

through its concomitant enrichment with S and C, is believed to be present as a combination of Cr sulfide and carbide (52). This depth profile and the quantitative analysis of the AES results (that the S content is approximately two monolayers) suggest that the structure of these segregands at the Al_2O_3/FeCrAl interfaces, illustrated by a simple schematic in **Figure 9*b***, is that of a S-rich top layer, followed by a second layer of mixed S, Cr, and C and then by a few underlayers enriched with Cr and C. Although so much S is present at these interfaces, the spallation resistance of Al_2O_3 scales formed on the MCrAl-type alloys is usually not worse than that found on NiAl or FeAl (80). This is due partly to the lower thermal expansion mismatch between α-Al_2O_3 and the MCrAl alloys (80) and also may be due partially to the relationship shown in **Figure 4**, in which the most dramatic decrease in interfacial strength is associated with the first ~0.2 monolayer of S coverage, and that excess S exhibits little effect. One other factor affecting Al_2O_3/MCrAl adhesion may be the bond-strengthening effect of Cr, which has been reported for a diffusion-bonded interface between Al_2O_3 and NiCr (81).

In summary, the effect of Cr addition in alloys is to increase the amount of S segregation at the scale/alloy interface due to cosegregation effects. This behavior, illustrated here with MCrAl-type alloys, also has been observed on NiPtAl-type coatings (48) and recently on γ/γ'-NiAl alloys. Without the addition of Cr, the interface S concentration on the binary Ni-22Al alloy is only ~3 at%. In contrast, with the presence of 5 at% Cr in the alloy, the S content increases to as high

as 10 at%, with a concomitant enrichment of Cr at the interface. As in the case of NiCrAl, C enrichment is not detected.

Reactive Element

It has been known for 70 years (82) that the presence of small amounts of REs in the alloy greatly improves Al_2O_3 scale adhesion. Although many mechanisms have been proposed to explain this phenomenon (83), the most widely accepted mechanism is the so-called S effect (6, 84). The hypothesis is that the oxide/metal interface is intrinsically strong, but indigenous S that is almost always present in alloys segregates to the interface during oxidation, thus weakening the bonding and rendering the scale nonadherent. The role of the REs, as a result of their strong sulfide-forming ability, is to tie up the S or, in other words, to reduce significantly the S activity in the alloy, preventing S segregation to the interface.

Indeed, when a RE is present in alloys, S is no longer detected at the Al_2O_3/alloy interface, where the detection limit by AES is usually <0.2 at% (or ~0.05–0.1 monolayer). This conclusion has been reached with Zr in Fe_3Al (85), Y in FeCrAlY (42, 43, 86), and Hf in β-NiAl and γ/γ′-NiAl. In all cases, Al_2O_3 scales formed on RE-containing alloys are also significantly more adherent. These results seem to corroborate the S effect hypothesis. Nevertheless, Al_2O_3/alloy interfaces that are S-free, i.e., those developed on H_2-annealed alloys that have been desulfurized, are noticeably weaker than those on RE-containing alloys. This has been demonstrated experimentally on desulfurized Fe_3Al (85, 87) and NiCrAl (88). Because many studies with STEM have shown that RE segregates at scale/alloy interfaces (see, e.g., Reference 89) and is at a level of 0.2–0.3 monolayer (90), the role of REs may be not only to prevent S from segregating to the interface but to exert a bond-strengthening effect there (85, 91). Earlier molecular orbital theory and large cluster models suggested strong bonding between alumina and Y (91). A recent first-principles calculation further demonstrated that the effect of Hf in γ-Ni(Al) is threefold (61). First, Hf pins S in the bulk and thus prevents S from segregating to the interface, as observed from the experiments noted above. Second, Hf also segregates at and strengthens the interface, which, again, agrees with experimental results. Lastly, Hf can displace S from interfacial sites.

When RE-containing alloys are heated in vacuum, S still segregates to the surface, although the amount is less than on the equivalent RE-free alloys (43, 92). In most cases, the REs themselves also segregate to the surface (92). Compared with segregation at oxide/alloy interfaces, the behavior is the same qualitatively, but not quantitatively. The difference is most likely due to limited sites at the oxide/alloy interface; it may also be related to different interface atomic structures that may have developed on alloys with or without REs. The presence of RE not only affects Al_2O_3 adhesion but also changes the Al_2O_3 oxide growth mechanism (93). This change in growth may affect the structure of the oxide/alloy interface in some ways so as to alter the chemical potential of the segregand at the interface. A similar structural dependence on segregation is common for alloy grain boundaries (62–64).

Platinum

The addition of Pt to an Al_2O_3 scale-forming alloy has been known since the mid-1970s to improve scale adhesion (94). Pt-modified NiAl is currently a common oxidation-resistant coating for high-temperature turbine engines (95), but the mechanism by which Pt exerts its beneficial effect is still not clear. If REs can improve Al_2O_3 scale adhesion by preventing S segregation to the interface owing to their high affinities for S, the same is not expected for Pt because Pt sulfide is even less stable than Al sulfide (96, 97). Perhaps Pt strengthens the interface by forming strong Pt-Al bonds,

Table 2 Surface concentrations of S, Al, and Pt at 750–1000°C by in situ AES or XPS

Alloy		Surface concentration (at%)		
Composition	S (ppmw)	S	Al	Pt
Ni-50Al[1]	4	0.3 ± 0.2	54.1 ± 0.8	
Ni-50Al-10Pt[1]		0	53.4 ± 1.5	17.6 ± 0.9
Ni-50Al[2]	57	5.9	65	
Ni-50Al-10Pt[2]	90	2.4	65	14
Ni-37Al[1]	3	8.7 ± 0.3	41.2 ± 0.8	
Ni-37Al-5Pt[1]		5.7 ± 0.9	41.0 ± 2.0	10.9 ± 0.6
Ni-25Al-10Pt(111)[3]		0	25.1 ± 0.3	17.3 ± 1.3
Ni-25Al-20Pt(111)[3]		0	25.8 ± 1.1	26.6 ± 2.2

[1]Hou & McCarty (56): analysis by AES at steady state, 1000°C.
[2]Cadoret et al. (100): analysis by XPS after 5 min heating at 750°C; S levels on NiAl and NiPtAl dropped to 3 and 1 at%, respectively, at steady state (after 60 min).
[3]Qin et al. (99): analysis by AES at steady state, 827°C.

because the binding energy between Pt and Al is stronger than that between Ni and Al (98). If this were the case, one would expect Pt to segregate to the Al_2O_3/Ni(Pt)Al interface. For these reasons, the segregation behaviors of Pt-containing NiAl alloys are of interest.

Several groups have studied the surface segregation behavior of Pt-containing NiAl alloys. These experiments were carried out by heating the alloy in vacuum, up to 750–1000°C, and then examining the surface composition at the high temperature, either with AES (56, 99) or XPS (100). **Table 2** summarizes the results. Each shaded color band compares two alloys made in the same laboratory, which differ only in their Pt content. Although the S level was not always evaluated, it is known that the amount of indigenous S in high-purity, laboratory-made NiAl and Ni(Pt)Al alloys is low, usually less than 4 ppm by weight (53, 100). The high-S NiAl and NiPtAl alloys studied by Cadoret et al. (100) were deliberately doped because the normal-purity alloys (with <1 ppm S) did not show any S surface segregation. Results from **Table 2** clearly show the following: (*a*) S segregation is more pronounced on Ni-rich β-NiAl than on stoichiometric NiAl, a result discussed in previous sections. (*b*) The amount of segregated S increases with increasing alloy S content, in accordance with segregation thermodynamics, represented by Equation 1. (*c*) Pt reduces the extent of S segregation to the surface. (*d*) Pt is enriched on the surface, whether the alloy is the stoichiometric or the Ni-rich β phase or the γ′ phase. (*e*) Some surfaces may also be enriched with Al.

First-principles calculations have shown that the segregation of Pt on the β phase is related to an increased surface energy, from 1.80 J m^{-2} to 2.44 J m^{-2}, when Pt is present in NiAl (101). For the γ′ phase, Qin et al. (99) postulated that the driving force for Pt segregation is the strain energy in the alloy resulting from the fact that Pt, residing on Ni lattice sites (101, 102), is larger than Ni. It remains unclear why S surface segregation is reduced by the presence of Pt. Hou & McCarty (56) suggested that this reduction may be due to a possible competition between Pt and S for surface sites.

The effect of Pt on interface segregation has not been studied as extensively. **Table 3** summarizes the existing results. On the stoichiometric Ni-50Al, with or without Pt addition, S is not detected at the interface above background levels under a wide range of oxidation conditions. With the Ni-rich β-NiAl, Pt in the alloy clearly stops S segregation to the interface. Unlike the case of segregation to free surfaces, Pt does not segregate to the Al_2O_3/β-NiAl interfaces. Al, in contrast, is enriched at Ni-40Al interfaces, making the composition of Ni-40Al similar to that of

Table 3 Composition of the alloy side of Al_2O_3/alloy interfaces determined by AES after oxide removal in UHV. The blue horizontal lines separate different compositions of β- and γ′- or γ/γ′-NiAl, the thick black horizonal line separates the β- and γ′-, γ/γ′-phases of the NiAl, and the gray shading highlights Pt-containing alloys

Alloy	Oxidation conditions	Interface concentration (at%)		
		S	Al	Pt
Ni-50Al	1000°C, 2–265 h	0.1 ± 0.1	54.7 ± 6.0	–
	1150°C, 100 h			
Ni-50Al-2.5Pt	1000°C, 26–100 h	0	64.1 ± 3.0	1.5 ± 1.4
Ni-50Al-15Pt	1150°C, 100 h	0	68.6 ± 5.6	12.1 ± 1.6
Ni-40Al	1000°C, 26–100 h	2.2 ± 0.5	54.2 ± 3.5	–
	1150°C, 3–100 h			
Ni-40Al-15Pt	1000°C, 100 h	0	54.8 ± 3.4	14.2 ± 1.9
	1150°C, 100 h			
Ni-25Al	1000°C, 24 h	0.2 ± 0.3	30.1 ± 2.1	
	1150°C, 20 h			
Ni-25Al-10Pt	1100°C, 50 h	0.5 ± 0.8	27.5 ± 3.6	15.5 ± 2.9
	1150°C, 100 h			
Ni-22Al	1150°C, 100 h	3.0 ± 0.7	28.8 ± 2.7	–
Ni-22Al-5Pt	1150°C, 100 h	1.4 ± 0.2	28.5 ± 3.3	12.2 ± 1.7

the stoichiometric NiAl. The presence of Pt in Ni-50Al seems also to increase the interfacial Al concentration. The variations in interface composition on the Pt-containing β-NiAl are further demonstrated by the AES depth profiles shown in **Figure 10**. No S is found; Al is enriched within a narrow region at the interface, and Pt may even be slightly depleted. The lack of S and the higher Al content at the interface both should, according to first-principles calculations (103),

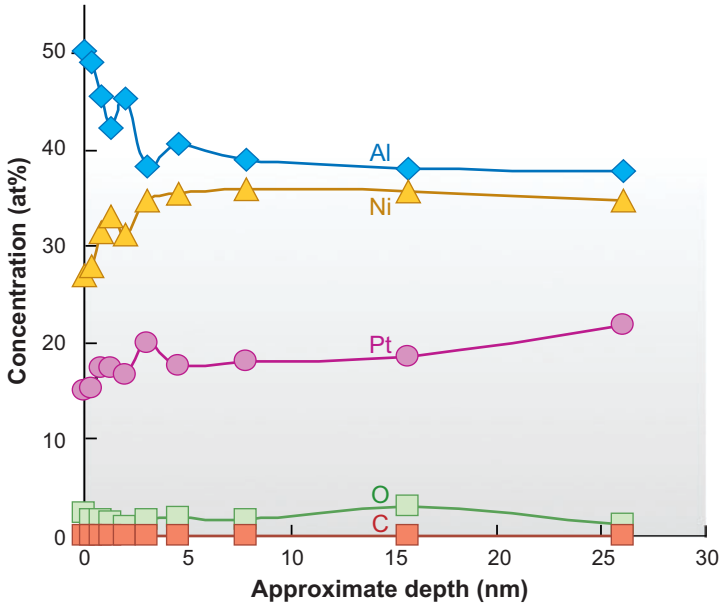

Figure 10

AES depth profiles through the surface of a Ni-40Al-15Pt alloy after its TGO was removed in UHV. The sample was oxidized at 1150°C for 100 h. S is not detected. The interface is enriched with Al, but not Pt.

increase the interface bond strength. Therefore, these interfacial chemical changes may be one way by which Pt exerts its beneficial effect on Al_2O_3 adhesion. On the γ'- and γ/γ'-NiAl, the segregation behavior becomes more similar to that on free surfaces, where Pt, but not Al, is enriched at the interface. As discussed above, the amount of S segregated at Al_2O_3/γ'-NiAl interfaces is barely above background. The alloy with Pt addition behaves the same. On the γ/γ'-NiAl, where ~3 at% S segregates to the interface, Pt in the alloy reduces, but does not eliminate, this segregation.

The mechanism by which Pt reduces interfacial S segregation in NiAl alloys and why this reduction varies with the alloy phase are not yet clear. It is also not known why Pt seems to be enriched at the interfaces between Al_2O_3 and γ- and γ'-NiAl, but not with β-NiAl. The data in **Table 3** suggest some degree of competitive segregation between Pt and Al at the interface. The effect of Pt on S segregation is certainly more complicated than the effect of Cr or REs. Compared with REs, the ability of Pt to stop S segregation seems weaker, whereas S and Cr cosegregation can overwhelm the effects of Pt. For example, although no S segregates at Al_2O_3/Ni-22Al-5Pt, almost 9% S is present at the interface when 5% Cr is added to the alloy owing to Cr cosegregation. NiPtAl coatings also exhibit cosegregation effects when Cr in the substrate diffuses into the coating and becomes enriched at the Al_2O_3/coating interface (48). In these systems, the presence of Pt is not able to reduce S segregation. It seems that whatever effect Pt has on ΔG_{seg} may be small, so that the segregation behavior can be easily dominated by the Ω_{12} term in Equation 1.

CONCLUSIONS

Segregation behavior at oxide/alloy interfaces during high-temperature oxidation is a topic in its infancy. Although the segregation of S to growing oxide/alloy interfaces is thermodynamic in nature, the segregation energy can change with oxidation time and temperature, perhaps depending mainly on the structure of the oxide/alloy interface. The situation is better understood for binary alloys, but even so, the effect of other common impurities, in particular C (104), needs to be, but has not been, considered. Although C does not segregate at growing oxide/alloy interfaces, its presence in the alloy may affect the activity of S and other elements, such as Cr and REs, hence affecting S segregation. The segregation phenomena with ternary or multicomponent alloys or coatings become even more complex. REs in the alloy have always been found to eliminate interfacial S segregation. Pt, so far studied only in NiAl, can also reduce this segregation, but the effect of Pt is less consistent. Synergisms between segregands can exist; an example is illustrated above for S and Cr in terms of cosegregation. Other interactions of alloying elements with potential segregands and with each other may be important as well. Furthermore, any alloying element that causes changes in interface energy, oxide growth mechanisms, and/or the activity of potential segregands in the alloy can also influence the nature of segregation. The relationships between these factors are not well established and should be investigated further.

SUMMARY POINTS

1. During high-temperature oxidation of Al_2O_3-forming alloys, at $T > 900°C$ S is the only nonmetallic impurity that consistently segregates at the growing interface; its presence weakens the interfacial strength.
2. S begins to segregate to Al_2O_3/FeAl and NiAl interfaces only when a complete layer of α-Al_2O_3 is developed. No S other than on interfacial void faces is detected when the interface is that between a transition alumina and the alloy.

3. With NiAl, S segregates to the interface only when the alloy is a disordered phase. Concentrations not much above background levels are found with ordered γ' or stoichiometric β alloys.
4. Small amounts of reactive elements (REs) (<0.1 at%) added in Ni- or Fe-based alloys prevent S segregation to the Al_2O_3/alloy interface, and the REs that segregate to interfaces further increase the interfacial strength.
5. S and Cr cosegregate to the interface, causing an increase in the interfacial S concentration. Pt eliminates S segregation at alumina/β-NiPtAl interfaces and reduces it when the alloy is the γ/γ' phase. The effect of Pt can be overwhelmed by the cosegregation of S with Cr.
6. The interfacial segregation process is thermodynamic in nature. The extent of segregation depends on the chemical potential of the solute in the alloy and at the interface, and interactions between the solute and other alloying elements. The segregation energy, however, tends to vary with time owing to the dynamic nature of the oxidation process.

FUTURE ISSUES

1. Owing to the dynamic nature of the TGO/alloy interfaces, segregation energy changes with time as the oxide evolves. Every oxide/alloy system may reach a steady state that can be characterized. However, many fundamental questions remain. For example, how does the structure of the oxide/alloy interface change with oxidation time, temperature, and alloying additions, and how do these changes affect interfacial segregation? Also, as oxidation progresses, the subscale alloy composition will change owing to inward and outward diffusion of different alloying elements, and this may alter the alloy phases. How do these variations affect segregation at the interface?
2. Because commercial alloys are often multicomponent, any synergism between alloying elements and potential segregands, other than that known for S and Cr, and S and REs, needs to be identified. The role of C-RE interaction in the alloy and how this interaction may affect S segregation or the ability of a RE to tie up S warrant more quantitative evaluation.
3. Further investigation, perhaps aided by first-principles calculations, is required to elucidate the effect of Pt, e.g., how Pt reduces S segregation to Al_2O_3/NiAl interfaces, and why the segregation process, for S as well as Pt, is different on different alloy phases.

DISCLOSURE STATEMENT

The author is not aware of any biases that might be perceived as affecting the objectivity of this review.

ACKNOWLEDGMENTS

Some of the alloys were provided by Drs. Bruce Pint and Peter Tortorelli at Oak Ridge National Laboratory and by Prof. Brian Gleeson at Iowa State University (now at the University

of Pittsburg). Hydrogen annealing of alloys was performed by Dr. James Smialek at NASA Glen Research Center. Some of the AES studies and the μXPS work were done, respectively, at the Molecular Foundry and the Advanced Light Source at Lawrence Berkeley National Laboratory. Financial support is provided by the Director, Office of Science, Office of Basic Energy Sciences, Materials Sciences and Engineering Division, of the U.S. Department of Energy under Contract No. DE-AC02-05CH11231.

LITERATURE CITED

1. Douben PA, Miller A, eds. 1990. *Surface Segregation Phenomena*. Boca Raton, FL: CRC Press. 1st ed.
2. Grabke HJ. 1989. Surface and grain boundary segregation on and in iron and steels. *ISIJ Int.* 29:529–38
3. Shin KS, Meshii M. 1983. Effect of sulfur segregation and hydrogen charging on intergranular fracture of iron. *Acta Metall.* 31:1559–66
4. Hippsley CA. 1987. Sulphur segregation and high-temperature brittle intergranular fracture in alloy steels. *Acta Metall.* 35:2399–416
5. Johnson WC, Blakely JM, eds. 1997. *Interfacial Segregation*. Metals Park, OH: ASM
6. Funkenbusch AW, Smeggil JG, Bornstein NS. 1985. Reactive element-sulfur interaction and oxide scale adherence. *Metall. Trans. A* 16:1164–66
7. Smialek JL. 1991. Effect of sulfur removal on Al_2O_3 scale adhesion. *Metall. Trans. A* 22:739–52
8. Smialek JL. 2000. Maintaining adhesion of protective Al_2O_3 scales. *JOM* 52:22–25
9. Grabke HJ, Wiemer D, Viefhaus H. 1991. Segregation of sulfur during growth of oxide scales. *Appl. Surf. Sci.* 47:243–52
10. Fox F, Lees DG, Lorimer GW. 1991. Sulfur segregation during the high-temperature oxidation of chromium. *Oxid. Met.* 36:491–502
11. Hou PY. 1998. Kinetics of sulfur segregation to scale-alloy interfaces. In *High Temperature Corrosion and Materials Chemistry*, ed. PY Hou, MJ McNallan, R Oltra, EJ Opila, DA Shores, 98–99:198–210. Pennington, NJ: Electrochem. Soc.
12. Hou PY, Stringer J. 1992. Oxide scale adhesion and impurity segregation at the scale/metal interface. *Oxid. Met.* 38:323–45
13. Papaiacovou P, Hussey RJ, Mitchell DF, Graham MJ. 1990. Interfacial segregation during oxidation in O_2 at 1173 K of CeO_2-coated Fe-20Cr alloys. *Oxid. Met.* 33:19–30
14. Brady MP, Pint BA, Tortorelli FP, Wright IG, Hanrahan RJ Jr. 2000. High temperature oxidation and corrosion of intermetallics. In *Corrosion and Environmental Degradation*, ed. M Schutze, 19:232–325. New York: Wiley-VCH
15. Giggins CS, Pettit FS. 1972. Oxidation of Ni-Cr-Al alloys between 1000° and 1200°C. *J. Electrochem. Soc.* 118:1782–90
16. Tomaszewicz P, Wallwork GR. 1983. The oxidation of high-purity iron-chromium-aluminum alloys at 800°C. *Oxid. Met.* 20:75–109
17. Rybicki GC, Smialek JL. 1989. Effect of the θ–α-Al_2O_3 transformation on the oxidation behavior of β-NiAl+Zr. *Oxid. Met.* 31:275–304
18. Hou PY, Paulikas AP, Veal BW. 2006. Stress development and relaxation in Al_2O_3 during early stage oxidation of β-NiAl. *Mater. High Temp.* 22:373–81
19. Doychak J, Rühle M. 1989. TEM studies of oxidized NiAl and Ni_3Al cross sections. *Oxid. Met.* 31:431–52
20. Brumm MW, Grabke HJ. 1992. The oxidation behaviour of NiAl. I. Phase transformations in the alumina scale during oxidation of NiAl and NiAl-Cr alloys. *Corros. Sci.* 33:1677–90
21. Yang JC, Nadarzinski K, Schumann E, Rühle M. 1995. Electron microscopy studies of NiAl/γ-Al_2O_3 interface. *Scr. Metall.* 33:1043–48
22. Pint BA, Treska M, Hobbs LW. 1997. The effect of various oxide dispersions on the phase composition and morphology of Al_2O_3 scales grown on β-NiAl. *Oxid. Met.* 47:1–20
23. Andoh A, Taniguchi S, Shibata T. 2001. TEM observation of phase transformations of alumina scales formed on Al-deposited Fe-Cr-Al foils. *Mater. Sci. Forum* 369–372:303–10

24. Doychak J, Smialek JL, Mitchell TE. 1989. Transient oxidation of single-crystal β-NiAl. *Metall. Trans. A* 20:499–518
25. Sigler DR. 1991. Oxidation behaviour of Fe-20Cr-5Al rare earth alloys in air and synthetic exhaust gas. *Oxid. Met.* 36:57–80
26. Zhang XF, Thaidigsmann K, Ager J, Hou PY. 2006. Alumina scale development on iron aluminides. *J. Mater. Res.* 21:1409–19
27. Schumann E, Rühle M. 1994. Microstructural observation on the oxidation of γ′-Ni_3Al at high oxygen partial pressure. *Acta Metall. Mater.* 42:1481–86
28. Yang JC, Schumann E, Müllejans H, Rühle M. 1996. Chemistry and bonding investigations of NiAl/γ-Al_2O_3 interfaces. *J. Phys. D* 29:1716–24
29. Hagel WC. 1965. The oxidation of iron, nickel and cobalt-based alloys containing aluminum. *Corrosion* 21:316–26
30. Renusch D, Grimsditch M, Koshelev I, Veal BW, Hou PY. 1997. Strain determination in thermally grown alumina scales using fluorescence spectroscopy. *Oxid. Met.* 48:471–95
31. Jedlinski J, Borchardt G, Mrowec S. 1992. Transport properties of alumina scales on the β-NiAl intermetallic. *Solid State Ionics* 50:67–74
32. Pint BA, Martin JR, Hobbs LW. 1995. The oxidation mechanism of θ-Al_2O_3 scales. *Solid State Ionics* 78:99–107
33. Prescott R, Mitchell DF, Graham MJ. 1994. A study of the growth of α-Al_2O_3 scales using high-resolution imaging secondary ion mass spectrometry. *Corrosion* 50:62–71
34. Mennicke C, Schumann E, Ruhle M, Hussey RJ, Sproule GJ, Graham MJ. 1998. The effect of yttrium on the growth process and microstructure of α-Al_2O_3 on FeCrAl. *Oxid. Met.* 49:455–66
35. Tortorelli PF, More KL, Specht ED, Pint BA, Zschack P. 2003. Growth stress-microstructure relationships for alumina scales. *Mater. High Temp.* 20:303–10
36. Hou PY, Paulikas AP, Veal BW. 2004. Growth strains and stress relaxation in alumina scales during high temperature oxidation. *Mater. Sci. Forum* 461–464:671–80
37. Brumm MW, Grabke HJ. 1993. Oxidation behaviour of NiAl. II. Cavity formation beneath the oxide scale on NiAl of different stoichiometries. *Corros. Sci.* 34:547–61
38. Hou PY, Niu Y, Van Lienden C. 2003. Analysis of pore formation at oxide/alloy interfaces. Part I. Experimental results on FeAl. *Oxid. Met.* 59:41–61
39. Rivoaland L, Maurice V, Josso P, Bacos MP, Marcus P. 2003. The effect of sulfur segregation on the adherence of the thermally grown oxide on NiAl. *Oxid. Met.* 60:137–57
40. Rouzou I, Molins R, Rémy R, Jomard F. 2004. Study of the sulfur segregation for a TBC system. *Mater. Sci. Forum* 461–464:101–8
41. Glazkov A, Gobel M, Borchardt G, Al-Badary H, Ritherdon J, et al. 1997. An Auger study of the composition of the metal/oxide interface in Fe-20Cr-5Al based alloys revealed by bending experiments under UHV conditions. In *Microscopy of Oxidation*, ed. JB Newcomb, JA Little, 3:105–14. London: Inst. Met.
42. Schmutzler HJ, Viefhaus H, Grabke HJ. 1992. The influence of the oxide/metal interface composition on the adherence of oxide layers on metal substrates. *Surf. Interface Anal.* 18:581–84
43. Tolpygo VK, Viefhaus H. 1999. Segregation at the Al_2O_3-FeCrAl interface during high-temperature oxidation. *Oxid. Met.* 52:1–29
44. Hou PY. 2000. Compositions at Al_2O_3/FeCrAl interfaces after high temperature oxidation. *Mater. Corros.* 51:329–37
45. Hou PY, Prüßner K, Fairbrother DH, Roberts JG, Alexander KB. 1999. Sulfur segregation to deposited Al_2O_3 film/alloy interface at 1000°C. *Scr. Mater.* 40:241–47
46. Prüßner K, Schumann E, Rühle M. 1997. Oxidation of S-doped β-NiAl in H_2/H_2O and in air. In *Proc. Symp. Fundam. Asp. High Temp. Corros.*, ed. DA Shores, RA Rapp, PY Hou, PV96-26:344–51. Pennington, NJ: Electrochem. Soc.
47. Molins R, Rouzou I, Hou PY. 2007. A TEM study of sulfur distribution in oxidized Ni40Al and its effect on oxide growth and adhesion. *Mater. Sci. Eng. A* 454–455:80–88
48. Molins R, Rouzou I, Hou PY. 2006. Chemical and morphological evolution of a (NiPt)Al bondcoat. *Oxid. Met.* 65:263–83

49. Smeggil JG, Funkenbusch AW, Bornstein NS. 1986. A relationship between indigenous impurity elements and protective oxide scale adherence characteristics. *Metall. Trans. A* 17:923–32
50. Yang S, Wang FH. 2006. Effect of nanocrystallization on sulfur segregation in Fe-Cr-Al alloy during oxidation at 1000°C. *Oxid. Met.* 65:195–205
51. Hou PY, Moskito J. 2003. Sulfur distribution on Al_2O_3/FeAl interfaces studied by field emission-Auger electron spectroscopy. *Oxid. Met.* 59:559–74
52. Hou PY, Ackerman GD. 2001. Chemical state of segregants at Al_2O_3/alloy interfaces studied using mXPS. *Appl. Surf. Sci.* 178:156–64
53. Hou PY, Priimak K. 2005. Interfacial segregation, pore formation and scale adhesion on NiAl alloys. *Oxid. Met.* 63:113–30
54. Hou PY. 2003. Chemical and morphological changes at Al_2O_3/NiAl interfaces and their relationship to scale adhesion. In *High Temperature Corrosion and Materials Chemistry, IV*, ed. E Opila, PY Hou, T Maruyama, B Pieraggi, M McNallan, et al., 2003-16:40–50. Pennington, NJ: Electrochem. Soc.
55. Briggs D, Seah MP, eds. 1990. *Practical Surface Analysis, Vol. 1: Auger and X-Ray Photoelectron Spectroscopy*. New York: John Wiley & Sons. 2nd ed.
56. Hou PY, McCarty KF. 2006. Surface and interface segregation in NiPtAl alloys. *Scr. Mater.* 54:937–41
57. Blum V, Schmid A, Meier W, Hammer L, Heinz K. 2003. Competitive surface segregation of C, Al and S impurities in Fe(100). *J. Phys. Condens. Matter* 15:3517–29
58. Mulford RA. 1983. Grain boundary segregation in Ni and binary Ni alloys doped with sulfur. *Metall. Trans. A* 14:865–70
59. de Plessis J. 1990. Surface segregation. *Diffusion and Defect Data. Part B. Solid State Phenomena*, 11:22–32. Brookfield, VT: Sci-Tech Publ.
60. Miyahara T, Stolt K, Read DA, Birnbaum HK. 1985. Sulfur segregation on Ni. *Scr. Metall.* 19:117–21
61. Smith JR, Jiang Y, Evans AG. 2007. Adhesion of the γ-Ni(Al)/α-Al_2O_3 interface: a first-principles assessment. *Int. J. Mater. Res.* 12:1214–21
62. Balluffi RW. 1997. Grain boundary structure and segregation. See Ref. 5, pp. 193–237
63. Rittner JD, Udler D, Seidman DN, Oh Y. 1995. Atomic scale structural effects on solute-atom segregation at grain boundaries. *Phys. Rev. Lett.* 74:1115–18
64. Rittner JD, Udler D, Seidman DN. 1996. Solute-atom segregation at symmetric twist and tilt boundaries in binary metallic alloys on an atomic-scale. *Interface Sci.* 4:65–80
65. Hou PY, Paulikas AP, Veal BW. 2006. Strains in thermally grown alumina films measured using in-situ synchrotron X-rays. *Mater. Sci. Forum* 522–23:433–40
66. Bonnell DA, Kiely J. 1998. Plasticity at multiple length scales in metal-ceramic interface fracture. *Phys. Status Solid. A* 166:7–17
67. Elssner G, Korn D, Rühle M. 1994. The influence of interface impurities on fracture energy of UHV diffusion bonded metal-ceramic bicrystals. *Scr. Metall. Mater.* 31:1037–42
68. Gaudette FG, Suresh S, Evans AG. 2000. Effect of sulphur on the fatigue and fracture resistance of interfaces between γ-Ni(Cr) and α-Al_2O_3. *Metall. Mater. Trans. A* 31:1977–83
69. Hou PY, Saunders A. 2005. A survey of test methods for scale adhesion measurement. *Mater. High Temp.* 22:121–30
70. Frank S, Divinski SV, Sodervall U, Herzig C. 2001. Ni tracer diffusion in the B2-compound NiAl: influence of temperature and composition. *Acta Mater.* 49:1399–411
71. Shelton JC, Patil HR, Blakely JM. 1974. Equilibrium segregation of carbon to a nickel (111) surface: a surface phase transition. *Surf. Sci.* 43:493–520
72. Isett LC, Blakely JM. 1976. Segregation isosteres for carbon at the (100) surface of nickel. *Surf. Sci.* 58:397–414
73. Levin ES, Ayushina GD, Gel'd PV. 1968. Density and surface-energy polytherms of liquid (molten) aluminum. *High Temp.* 6:416–18
74. Gessinger GH, Singer RF. 1983. Superalloys: principles and applications. In *Deformation of Multi-Phase and Particle Containing Materials*, ed. JB Bilde-Sorensen, N Hansen, A Horsewell, T Leffers, H Liholt, pp. 15–26. Roskilde, Den.: Riso Natl. Lab.

75. L'nyanoi VN. 1999. Carbon diffusion in Ni-C, Co-C, and Fe-C alloys. *Metally* 1:119–22
76. Kochubey V, Naumenko D, Wessel E, Le Coze J, Singheiser L, et al. 2006. Evidence for Cr-carbide formation at the scale/metal interface during oxidation of FeCrAl alloys. *Mater. Lett.* 60:1654–58
77. Uebing C. 1996. Surface cosegregation phenomena on alloys and steels: structural features and phase transitions. *Prog. Surf. Sci.* 53:297–304
78. Uebing C. 1990. Formation of surface compounds on Fe–15% Cr{100} single crystals. *Surf. Sci.* 225:97–106
79. Dziakova A, Clauberg E, Uebing C, Janovec J. 1999. Surface cosegregation of chromium and sulfur in single crystalline austenitic Fe-Ni-Cr alloys. *Surf. Rev. Lett.* 6:389–97
80. Haynes JA, Pint BA, Porter WD, Wright IG. 2004. Comparison of thermal expansion and oxidation behavior of various high-temperature coating materials and superalloys. *Mater. High Temp.* 21:87–94
81. Gaudette F, Suresh S, Evans AG, Dehm G, Rühle M. 1997. The influence of chromium addition on the toughness of γ-Ni/α-Al_2O_3 interfaces. *Acta Mater.* 45:3503–13
82. Pfeil LB. 1937. Improvement in heat-resisting alloys. *U.K. Patent No. 459,848*
83. Whittle DP, Stringer J. 1980. Improvements in high temperature oxidation resistance by additions of reactive elements or oxide dispersions. *Philos. Trans. R. Soc. London* 295:309–29
84. Lees D. 1987. On the reasons for the effects of dispersions of stable oxides and additions of reactive elements on the adhesion and growth-mechanisms of chromia and alumina scales: the "sulfur effect." *Oxid. Met.* 27:75–92
85. Hou PY. 1999. Beyond the sulfur effect. *Oxid. Met.* 52:337–51
86. Mennicke C, Schumann E, Al-Badairy H, Tatlock GJ, Goebel M, et al. 1998. High temperature oxidation of UHP-based Fe20Cr5Al alloys. *Phys. Status Solid. A* 167:419–26
87. Hou PY, Paulikas AP, Veal BW, Smialek JL. 2007. Thermally grown Al_2O_3 on a H_2-annealed Fe_3Al alloy: stress evolution and film adhesion. *Acta Mater.* 55:5601–13
88. Hou PY. 2003. Segregation phenomena at growing alumina/alloy interfaces. *J. Corros. Sci. Eng.* 6:paper 75
89. Pint BA, Alexander KB. 1998. Grain boundary segregation of cation dopants in α-Al_2O_3 scales. *J. Electrochem. Soc.* 145:1819–29
90. Schumann E, Yang JC, Graham MJ, Rühle M. 1995. Segregation studies of oxidized Y and Zr doped NiAl. *Werkst. Korros.* 46:218–22
91. Anderson AB, Mehandru SP, Smialek JL. 1985. Dopant effect of yttrium and the growth and adherence of alumina on nickel-aluminum alloys. *J. Electrochem. Soc.* 132:1695–701
92. Briant CL, Luthra KL. 1988. Surface segregation in MCrAlY alloys. *Metall. Trans. A* 19:2099–108
93. Pint BA. 2001. Progress in understanding the reactive element effect. In *Proc. John Stringer Symp. High Temp. Corros.*, ed. P Tortorelli, IG Wright, PY Hou, pp. 52–62. Metals Park, OH: ASM Int.
94. Felten EJ. 1976. Use of platinum and rhodium to improve oxide adherence on Ni-8Cr-6Al alloys. *Oxid. Met.* 10:23–28
95. Schmitt-Thomas KG, Hertter M. 1999. Improved oxidation resistance of thermal barrier coatings. *Surf. Coat. Tech.* 120–121:84–88
96. Sigler DR. 1989. Aluminum oxide adherence on Fe-Cr-Al alloys modified with group IIIB, IVB, VB and VIB elements. *Oxid. Met.* 32:337–55
97. Lide DR. 2001–2002. *Handbook of Physics and Chemistry*. Boca Raton, FL: CRC Press. 82nd ed.
98. Mayer M, Pacchioni G, Rosch N. 1998. Bonding of transition metal atoms on the Al(100) surface from density functional calculations. *Surf. Sci.* 412/413:616–24
99. Qin F, Jiang C, Anderegg JW, Jenks CJ, Gleeson B, et al. 2007. Segregation of Pt at clean surfaces of $(Pt, Ni)_3Al$. *Surf. Sci.* 601:376–80
100. Cadoret Y, Bacos M-P, Josso P, Maurice V, Marcus P, Zanna S. 2004. Effect of Pt additions on the sulfur segregation, void formation and oxide scale growth of cast nickel aluminides. *Mater. Sci. Forum* 461–64:247–54
101. Yu R, Hou PY. 2007. First principles calculation of the effect of Pt on NiAl surface energy. *Appl. Phys. Lett.* 91:011907

102. Jiang C, Besser MF, Sordelet DJ, Gleeson B. 2005. A combined first-principles and experimental study of the lattice site preference of Pt in B2 NiAl. *Acta Mater.* 53:2101–9
103. Zhang W, Smith JR, Wang X-G, Evans AG. 2003. Influence of sulfur on the adhesion of the nickel/alumina interface. *Phys. Rev. B* 67:245414
104. Pint BA, Schneibel JH. 2005. The effect of carbon and reactive element dopants on oxidation lifetime of FeAl. *Scr. Mater.* 52:1199–204